Biomacromolecules

pubs.acs.org/Biomac

Article

Three-Dimensional Printed Cell Culture Model Based on Spherical Colloidal Lignin Particles and Cellulose Nanofibril-Alginate Hydrogel

Xue Zhang, Maria Morits, Christopher Jonkergouw, Ari Ora, Juan José Valle-Delgado, Muhammad Farooq, Rubina Ajdary, Siqi Huan, Markus Linder, Orlando Rojas, Mika Henrikki Sipponen, and Monika Österberg*

Cite This: *Biomacromolecules* 2020, 21, 1875−1885

Read Online

ACCESS | Metrics & More | Article Recommendations | Supporting Information

ABSTRACT: Three-dimensional (3D) printing has been an emerging technique to fabricate precise scaffolds for biomedical applications. Cellulose nanofibril (CNF) hydrogels have attracted considerable attention as a material for 3D printing because of their shear-thinning properties. Combining cellulose nanofibril hydrogels with alginate is an effective method to enable cross-linking of the printed scaffolds in the presence of Ca^{2+} ions. In this work, spherical colloidal lignin particles (CLPs, also known as spherical lignin nanoparticles) were used to prepare CNF-alginate-CLP nanocomposite scaffolds. High-resolution images obtained by atomic force microscopy (AFM) showed that CLPs were homogeneously mixed with the CNF hydrogel. CLPs brought antioxidant properties to the CNF-alginate-CLP scaffolds in a concentration-dependent manner and increased the viscosity of the hydrogels at a low shear rate, which correspondingly provide better shape fidelity and printing resolution to the scaffolds. Interestingly, the CLPs did not affect the viscosity at high shear rates, showing that the shear thinning behavior typical for CNF hydrogels was retained, enabling easy printing. The CNF-alginate-CLP scaffolds demonstrated shape stability after printing, cross-linking, and storage in Dulbecco's phosphate buffer solution (DPBS +) containing Ca^{2+} and Mg^{2+} ions, up to 7 days. The 3D-printed scaffolds showed relative rehydration ratio values above 80% after freeze-drying, demonstrating a high water-retaining capability. Cell viability tests using hepatocellular carcinoma cell line HepG2 showed no negative effect of CLPs on cell proliferation. Fluorescence microscopy indicated that HepG2 cells grew not only on the surfaces but also inside the porous scaffolds. Overall, our results demonstrate that nanocomposite CNF-alginate-CLP scaffolds have high potential in soft-tissue engineering and regenerative-medicine applications.

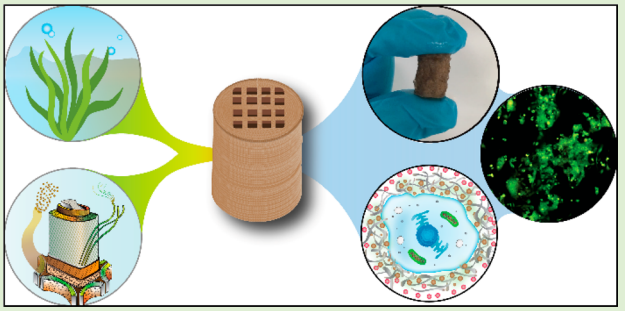

INTRODUCTION

There is a growing interest to manufacture three-dimensional (3D) cell culture models.[1] The reasons behind this interest are the many advantages of 3D cell culture over conventional two-dimensional culture. The 3D cell culture models have physicochemical properties resembling the native microenvironment of the cells, leading to more natural cell shape, possibility of cell−cell interaction, and cell behavior more similar to the ones in a physiological condition.[2,3] All of the above properties are advantageous for studies of disease mechanisms, the development of drug therapeutics, and tissue reconstruction. Hydrogels have attracted interest as materials for producing 3D cell culture models.[4,5] The physical properties of the hydrogels, such as mechanical properties, dimensional stability, and rehydration degree play vital roles in the potential applications.[4] Mechanical properties, particularly stiffness, regulate cellular processes such as proliferation, cell spreading, and cell differentiation via different mechanotransduction mechanisms.[6] A variety of materials have been used for the preparation of hydrogels, such as synthetic polymers like poly(ethylene glycol), poly(vinyl alcohol), and poly(2-hydroxy ethyl methacrylate) and natural polymers like collagen, fibrin, hyaluronic acid, chitosan, alginate, and cellulose nanofibrils (CNFs).[4,7] CNF is a nanomaterial derived from wood (and other plants) by mechanical disintegration. It has micrometer-long flexible fibrils with a thickness in the nanometer range.[8] CNF hydrogels are attractive materials for biomedical applications because they are nontoxic, xeno-free, biocompatible, and abundant.[9,10] The high water-binding ability and structural resemblance to the natural extracellular matrix make CNF an interesting material for 3D cell cultures.[7,11,12]

As an emerging additive manufacturing technique, 3D printing enables various architectures which makes it an attractive method for tissue engineering.[13,14] High printability

Special Issue: Anselme Payen Award Special Issue

Received: December 18, 2019
Revised: January 24, 2020
Published: January 29, 2020

https://dx.doi.org/10.1021/acs.biomac.9b01745
Biomacromolecules 2020, 21, 1875−1885

and mechanical stability of the scaffolds are essential properties for the biomaterial inks to be used. The inherent shear-thinning properties and biocompatibility make CNF hydrogels well-suited for 3D printing. However, CNF hydrogels possess poor mechanical properties, and pure CNF scaffolds tend to collapse upon drying.[15] There are different approaches for the post-treatment in order to tune the mechanical properties of CNF-based scaffolds, the most common one being cross-linking. In order to enable cross-linking of CNF-based scaffolds, their composition can be supplemented by physically cross-linkable components like collagen I,[16] copolymers of dimethylacrylamide[17] and alginate,[18] or chemically cross-linkable components like starch, isocyanates, and xylan−tyramine.[19,20] However, it has to be pointed out that chemical cross-linking can have a negative impact on cellular viability. The stability of CNF-based scaffolds can be further improved by the preparation of emulsion gel inks using polylactide.[21]

There are two approaches to 3D print scaffolds for tissue engineering: 3D bioprinting refers to 3D printing of cell-laden inks requiring cell-compatible conditions of printing and tuning the mechanical properties of printed scaffolds while another common method is the printing of scaffolds using biomaterial inks (i.e., natural biocompatible hydrogels and then seeding the scaffolds with cells after printing).[22] Alginate-containing bioinks have recently received considerable attention in the field of 3D bioprinting.[23] A major advantage of alginate solutions, along with their biocompatibility, biodegradability, nonimmunogenicity, abundance, and sustainability,[24] is the fast cross-linking by chelation in the presence of multivalent cations such as Ca^{2+} and Mg^{2+}. CNF-alginate gels have proven to be suitable formulations for the preparation of both biomaterial inks and bioinks.[18] It has been demonstrated that Ca^{2+} ions can effectively cross-link printed scaffolds made of CNF and alginate[18] because of the negatively charged carboxyl groups of alginate that provide abundant cross-linking sites for multivalent cations.[25] Equally important, the CNF-alginate scaffold demonstrated biocompatibility and suitability for cell culture.[18] However, there remains room for improvement in the functionalities of this composition as explained below.

New components with novel properties can be added to enrich the properties of CNF-alginate biomaterial inks. For biomedical applications, the new components should fulfill the requirements of biocompatibility, sustainability, and preferably low cost. Lignin, a complex phenolic polymer, stands out among a variety of plant-based materials because of its combination of antioxidant and antimicrobial activities and UV-shielding properties, besides its abundance and low cost.[26,27] Annually, 50−70 million tons of lignin is produced as a byproduct from pulping and lignocellulosic bioethanol industries.[26] It has been shown that the antioxidant and antimicrobial activities of lignin can prevent wound inflammation; lignin nanofibers, in particular, enable moisture retention and promote wound-healing capability of wound-dressing hydrogels.[28] In addition, the various different functional groups of lignin, like hydroxyl, methoxyl, carbonyl, and carboxylic groups, offer multiple sites for chemical modifications and thus broaden its potential applications.[29,30] All these advantages make lignin interesting as a component of tissue scaffolds.[27,31] Nevertheless, lignin-based materials have not received sufficient attention as materials for 3D cell culture. Earlier related research deals with hydrogels,[32] aerogels,[31] and electrospinning of microfibers,[33] while lignin has rarely been studied as a component of a printable polymer system for melt-extrusion 3D printing in biomedical applications.[34] The lack of reports using lignin for cell culturing materials may be due to the low water-solubility and chemical heterogeneity of common technical lignins that are predominantly available from the kraft pulping process.

Among the different lignin-based materials, colloidal lignin particles, also termed as lignin nanoparticles (LNPs), overcome the problems of low water-solubility and heterogeneity of kraft lignins.[35−37] CLPs have been studied extensively in recent years.[36−38] In the biomedical field, CLPs demonstrated great potential as gene- and drug-carrier systems,[39] antimicrobial[40] and wound-sealing materials,[41] adhesives, and hydrogels.[42] For instance, hydrogels containing silver-lignin nanoparticles showed good cell affinity and tissue adhesiveness; therefore, they are a promising material for wound healing.[42] We expect that CLPs hold untapped benefits for 3D bioprinting because of their antimicrobial and antioxidant properties, for example. These properties are especially useful in wound-healing applications and in general for storage of the material (with or without drugs incorporated). Their well-defined surface chemistry is, furthermore, suitable for a variety of surface modifications enabling optimization of cell adhesion. CLPs can be coated with proteins that are used in cell culture such as gelatin and poly-L-lysine,[43] and CLPs can also carry entrapped bioactive molecules such as pharmaceuticals.[44,35]

The goal of the current work was to explore the feasibility of using CLPs as a functional ingredient of biomaterial inks for 3D printing and further seeding with cells. A series of homogeneous CNF−alginate−CLP biomaterial inks were prepared and characterized for applications in 3D printing. Characterization included rheological properties, morphology by atomic force microscopy (AFM), and antioxidant activity of biomaterial inks. To demonstrate the positive effect of CLPs on printing resolution and shape fidelity, we designed a 2 cm high 3D model of a scaffold with thin grids. Scaffolds of various compositions were fabricated using a 3D printer. Aiming for biomedical application, the mechanical properties and water retaining capability of the scaffolds as well as their shape stability under different conditions including storage in Dulbecco's phosphate buffer solution (DPBS+) buffer solution were studied. To demonstrate the biocompatibility of the materials in the body, the viability of hepatocellular carcinoma cell line HepG2 cells was shown. To our knowledge, this is the first report on the advantages of CLPs for 3D-printing and tissue engineering.

MATERIALS AND METHODS

Materials. Softwood Kraft Lignin powder (UPM BioPiva™ 100) purified by the LignoBoost process was used in the present research. For detailed characterization of the lignin, see Sipponen et al.[45] Never-dried, bleached kraft birch pulp was used to prepare CNF. Unless otherwise stated, all other chemicals and solvents were purchased from Sigma-Aldrich, Gibco, or Corning and were used without any further purification.

Preparation and Characterization of Colloidal Lignin Particles (CLPs). Kraft lignin powder (5 g) was dissolved in 90 g of acetone/water 3:1 (w/w) mixture and stirred for 3 h at room temperature. The lignin solution was then filtered using a glass fiber (GF/F Whatman, pore size 0.7 μm) to discard the undissolved aggregates. Then 270 g of water was poured rapidly into the filtered solution. The resulting CLPs dispersion was placed in dialysis tubes (Spectra/Por dialysis membrane, pore size 6−8 kDa) and dialyzed against water for 2 days to remove acetone and low-molecular-weight

https://dx.doi.org/10.1021/acs.biomac.9b01745
Biomacromolecules 2020, 21, 1875−1885

Scheme 1. Schematic Illustration of Biomaterial Ink Preparation and 3D Printing[a]

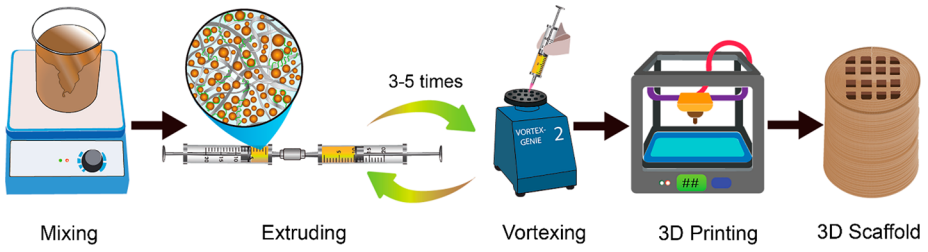

[a]Note: not drawn to scale.

impurities. Afterward, the dispersion was concentrated under reduced pressure at 45 °C, followed by filtration using VWR qualitative filter paper, 415 (particle retention 12−15 μm). The final concentration of CLPs dispersion was 3.83 wt %. The particle size distribution and zeta potential of CLPs dispersion was measured by a Zetasizer NanoZS90 instrument (Malvern Instruments Ltd. U.K). The average size of CLPs was 244 ± 4 nm, and the average zeta potential was −37 ± 3 mV.

Preparation of Cellulose Nanofibril (CNF) Hydrogel. CNF was prepared by the procedure described previously by Eronen et al.[46] Briefly, never-dried, bleached kraft birch pulp was fibrillated by applying a type M-110P microfluidizer (Microfluidics, Newton, MA), with 6 passes through the microfluidizer (Microfluidics, Newton, MA). No further treatments were done prior to fibrillation. The final dry matter of the CNF solution was 2.71 wt %. The CNF hydrogel was kept at +4 °C until use.

Preparation of 3D Printing Biomaterial Inks. Biomaterial inks for 3D printing were prepared from CNF and sodium alginate (Sigma-Aldrich) with a different content of CLPs. The procedure is shown in Scheme 1. A CLP dispersion was first mixed with alginate powder and stirred overnight. CNF was then mixed with the CLP−alginate dispersion by extrusion and vortex mixing. Five formulations of biomaterial inks were prepared (Table 1). Dry contents of CNF and alginate were kept at 2 and 0.5 wt %, respectively, for the five formulations. The weight ratio of CLP to CNF varied from 0 to 25 wt %. To remove air bubbles, the biomaterial inks were centrifuged at 2000 rpm for 2 min.

Table 1. Summary of Biomaterial Inks Formulations Used in This Work

biomaterial ink formulations	CLPs/CNF ratio	concentration in final ink (wt %)			
sample	% (w/w)	CLPs	CNF	Na-alginate	water content
CNFCLP0	0	0	2	0.5	97.50
CNFCLP1	1	0.02	2	0.5	97.48
CNFCLP5	5	0.10	2	0.5	97.40
CNFCLP10	10	0.20	2	0.5	97.30
CNFCLP25	25	0.50	2	0.5	97.00

Atomic Force Microscopy. A MultiMode 8AFM connected to a Nanoscope V controller (Bruker, Santa Barbara, CA) was utilized to obtain high-resolution images of CNF-alginate-CLP dry film topography. Biomaterial inks of all formulations were spread on a mica surface and air-dried. Films were imaged in ScanAsyst mode in air with a J scanner using ScanAsyst-air probes (Bruker AFM probes, Camarillo, CA) to check the homogeneity of CNF-alginate-CLP biomaterial inks. The obtained images were analyzed by NanoScope Analysis 1.5 software (Bruker). Flattening was the only image correction applied.

Antioxidant Activity of Biomaterial Inks. 2,2′-Azino-bis (3-ethylbenzothiazoline-6-sulfonic acid) cation radical (ABTS•+) was used to measure the antioxidant activity of biomaterial inks. The adapted procedure was described previously by Farooq et al.[47] Briefly, ABTS (Sigma-Aldrich) was dissolved in water to a 10 mM concentration. ABTS radical cation (ABTS•+) was produced by reacting ABTS (7 mM final concentration) with sodium persulfate (Sigma-Aldrich 2.45 mM final concentration). The mixture was stored in the dark at RT for 12−16 h before use. A freshly prepared 7 mM ABTS•+ stock solution was diluted with water until reaching an absorbance of 0.71 at a wavelength of 734 nm, at 25 °C. Biomaterial ink films were made by casting 3 times diluted biomaterial ink in Petri dishes and drying at 23 °C with 50% relative humidity for 4 days. Each film was placed in 2 mL of ABTS•+ solution. Samples were protected from light and were stirred using a Stuart tube rotator SB2 for 1 h. For calibration, 20 μL aliquots of tannic acid (Sigma-Aldrich) in the range of 0.01−0.25 mg/mL in water, was mixed with 2 mL of ABTS•+. The absorbance of solutions was measured at 734 nm exactly 1 h after mixing. To calculate the reduction of absorbance, the absorbance of ABTS•+ solution was measured after 1 h of preparation as standard. Composite films were measured in triplicates and tannic acid standards in duplicates. Mean values were reported as tannic acid equivalents (TAE) relative to the dry weight of the film sample, in mg/g. The absorbance of solutions was recorded on a UV−vis spectrophotometer (Shimadzu UV-2550).

Rheology. The rheological properties of the biomaterial inks were measured by a Physica MCR 301 rheometer (Anton-Paar) with a cone−plate geometry (Ø 50 mm and 1°). Shear viscosity data was recorded with a shear rate ranging from 0.01 to 100 s^{-1}. To evaluate the strength of the hydrogels, oscillation strain sweeps from 0.01% to 100% at a frequency of 1 Hz were performed to define the linear viscoelastic region (LVR). A strain of 0.1% was found to be within the LVR of all tested hydrogels. The oscillation frequency measurements were conducted between 0.01 and 650 rad/s, while the strain was kept constant at 0.1%.

3D Printing. The biomaterial inks were printed with a BIOX 3D printer (Cellink, Sweden). A pneumatic head connected to a 3 mL cartridge (CSC010311101) equipped with a standard blunt 22 needle tip (NZ5220505001) was used for printing all scaffolds. All scaffolds were printed at a speed of 11.5 mm/min with an infill density of 28%, unless stated otherwise. G-code files for printing were designed by either OpenSCAD or Thinkercad software.

For the shape-fidelity study, cylindrical scaffolds of each formulation with a diameter of 1.5 cm and a height of 2 cm were printed on polypropylene Petri dishes. The scaffolds were cross-linked by dipping in 90 mM of aqueous calcium chloride ($CaCl_2$), whereupon the scaffolds were stored at ambient conditions for 2 h or in 1× DPBS+ solution for 1 week at 4 °C. The non-cross-linked scaffolds were stored at ambient conditions for 2 h after printing.

For rehydration experiments, scaffolds with a diameter of 1.5 cm and height of 3 mm were printed and stored in 1× DPBS+ for 24 h (in this case, no additional $CaCl_2$ was used for cross-linking). For unconfined compression tests, constructs with a diameter of 1.5 cm and a height of 3 mm were printed with an infill density of 100%. Biocompatibility tests were performed on scaffolds printed directly into 12-well plate with a diameter of 8 mm and a height of 3 mm. Samples were incubated in 1× DPBS+ and stored at 4 °C overnight before testing.

Shape Fidelity and Rehydration Tests on Printed Scaffolds. The dimensional changes of printed scaffolds were measured under

https://dx.doi.org/10.1021/acs.biomac.9b01745
Biomacromolecules 2020, 21, 1875−1885

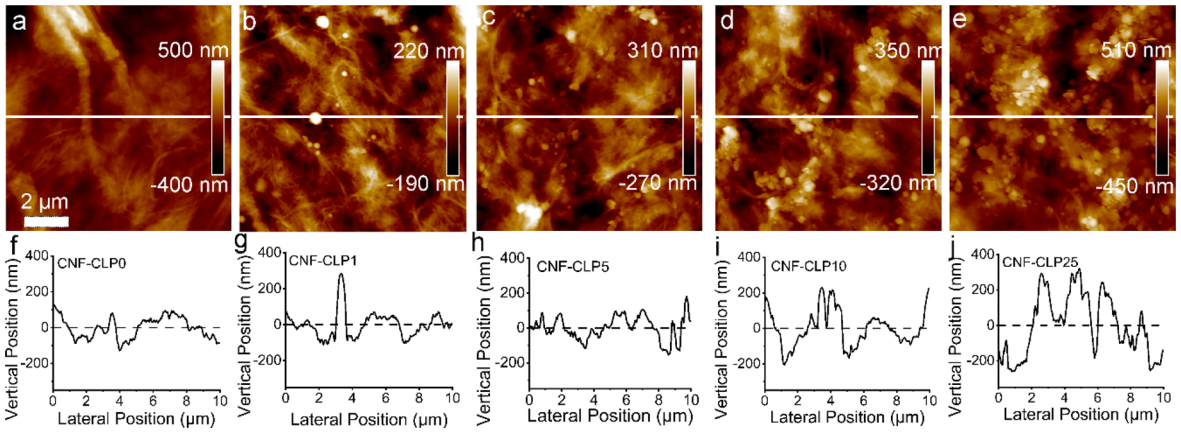

Figure 1. AFM height images of dry films of (a) CNF-CLP0, (b) CNF-CLP1, (c) CNF-CLP5, (d) CNF-CLP10, (e) CNF-CLP25, and the corresponding cross-section profiles (f–j). The cross-sectional profiles correspond to the white lines in (a–e) respectively. Scale bar, 2 μm.

three conditions, which include the storage of non-cross-linked samples, the storage of cross-linked samples at ambient conditions for 2 h, and the storage of cross-linked samples in 1× DPBS+ solution for 1 week at 4 °C. For the determination of dimensional changes of scaffolds, the height and cross-section of samples were measured before and after storage. In the case of non-cross-linked scaffolds, the height and cross-section measured immediately after 3D printing were used as reference (0% change), and in the case of cross-linked samples, the height and cross-section measured immediately after taking the samples out from the cross-linking bath containing 90 mM of aqueous $CaCl_2$ were used as reference. A minimum of two scaffolds for each formulation were tested for each condition.

The swelling properties were checked by conducting freeze-drying and rewetting. Scaffolds were freeze-dried at −46 °C, followed by soaking in Milli-Q water for 2 h until a swelling saturation state was reached. The dry weight and wet weight were measured. The swelling ratio and the rehydration ratio were calculated according to the following equations:

$$\text{swelling ratio} = \frac{W_1}{W_2}$$

$$\text{relative rehydration ratio} = \frac{W_3}{W_1}$$

where W_1 is the initial wet weight of the printed scaffolds, W_2 is the dry weight after freeze-drying, and W_3 is the wet weight after soaking in water for 2 h.

Unconfined Compression. Compression tests were performed on printed scaffolds with a diameter of 1.5 cm and a height of 3 mm which had been stored in 1× DPBS+ for 24 h at 4 °C. Initial dimensions of the cross-linked scaffolds were measured with a digital caliper. A universal testing machine (Instron 5944) equipped with a 50 N load cell was utilized for the unconfined compression test. The compression speed was set to 1 mm/min. Compressive stress and compressive strain were calculated with Bluehill software (Instron).

Biocompatibility. The scaffolds for biocompatibility tests were printed into 12-well plates. After the scaffolds were incubated overnight in 1× DPBS+ at 4 °C, they were put into a laminar flow cabinet (KOJAIR Biowizard Silver SL-130 Blue Series) and sterilized under UV light for 25 min. HepG2 cells were obtained from Biohybrid Materials Research Group, Aalto University. Two milliliters of HepG2 cells with a density of 3×10^5 cells/ml cultured in cell culture medium (Gibco, 41966–029) supplemented with 10% fetal bovine serum (Gibco, 10270–106) and 1% of penicillin and streptomycin (Sigma-Aldrich, 329820056) was seeded on each scaffold.

In vitro cytotoxicity testing and proliferation testing were performed using a WST-1 kit (Sigma-Aldrich, 11644807001) according to the supplier's manual. Cells were cultured for 1, 2, 3, and 5 days, after which the scaffolds were washed with PBS (Corning, 21-040-CV). Two milliliters of cell medium and 200 μL of WST-1 reagent were added to each scaffold-containing well. After 2 h of incubation, the assay solution (containing the formazan solution) was transferred into a new 96-well plate with a volume of 100 μL for each well, and the optical density (OD) was read at 460 nm using a Synergy H1 multimode microplate reader (Biotek, Bad Friedrichshall, Germany). To subtract the background, the same amount of cell medium and scaffolds for each formulation without cells was tested in the same way.

The initial cell viability before seeding the cells on the scaffolds was determined by trypan-blue (Gibco, 15250-061) staining (1:1 volumetric ratio). The viability was read by an automatic cell counter (Countess, Invitrogen). Cell viability was also tested on all the formulated scaffolds by fluorescence microscopy using a cell-permeable green fluorescent dye, calcein AM (148504-34-1, Sigma-Aldrich), and a cell-impermeable red fluorescent dye, propidium iodide (PI, Molecular Probes, 1159296, Thermo Fisher Scientific), to differentiate between dead and living cells. Scaffolds incubated with cells for 1, 3, and 5 days were washed with PBS once and incubated with 0.5 v/v% calcein AM and 0.25 v/v% PI in PBS for 20 min in a cell incubator. Both phase contrast and fluorescent images were acquired with an Axio Observer Z1 microscope (Carl Zeiss, Jena, Germany), equipped with an iXon Ultra 888 EMCCD camera (Andor Technology, Belfast, United Kingdom) and automated stage. Images were captured with a 10× 0.3 Ph1 objective, using a 1.6 optovar. The green fluorescent signal from calcein AM was obtained by an excitation window of 475–495 nm and collection of emission of 515–535 nm. The red fluorescent signal from PI was obtained by an excitation window of 502–517 nm and collection of emission of >615 nm (long pass filter). Images were further processed with Zen2 blue and ImageJ.

RESULTS AND DISCUSSION

Morphology of Biomaterial Inks. A high degree of homogeneity of biomaterial ink is crucial for 3D printing. Therefore, effort was made to develop an efficient method to mix thick CNF hydrogel and highly concentrated CLPs dispersion. A combined extruding and shaking technique was optimized to prepare homogeneous biomaterial inks. As shown in Scheme 1, biomaterial inks were extruded from one syringe to another with a connector in between and then shaken on a vortex. The whole procedure was repeated 3 to 5 times. Extruding the ink through the syringe adaptor decreased the viscosity of the CNF, enabling efficient mixing with alginate and CLPs. The continuous vortexing-induced shaking further increased the mixing of the three components in the hydrogel, assisting in the homogeneous dispersion of CLPs and alginate

https://dx.doi.org/10.1021/acs.biomac.9b01745
Biomacromolecules 2020, 21, 1875–1885

in the CNF hydrogel. The fibrillar network structure observed in the AFM height image (Figure 1a) of CNF-alginate biomaterial ink complies with the reported morphology of CNF.[48] The thickness of a single alginate strand is 1.41−4.65 nm;[49] thus, it is difficult to distinguish alginate from CNF. The added CLPs were observed as spheres evenly distributed within the fibril network, revealing that the CLPs were sufficiently well-dispersed in the CNF-alginate hydrogel (Figure 1b−e).

Rheological Properties of the Biomaterial Inks. The shear-thinning behavior is an essential property of biomaterial inks. Dynamic viscosity measurements revealed that all formulated series of CNF-alginate-CLPs bioinks demonstrated shear-thinning behavior well in accordance with previously reported behavior of CNF-alginate hydrogels without lignin.[18] The addition of CLPs did not alter the shear-thinning behavior, indicating that the series of CNF-alginate-CLPs biomaterial inks are suitable for bioprinting (Figure 2a). The

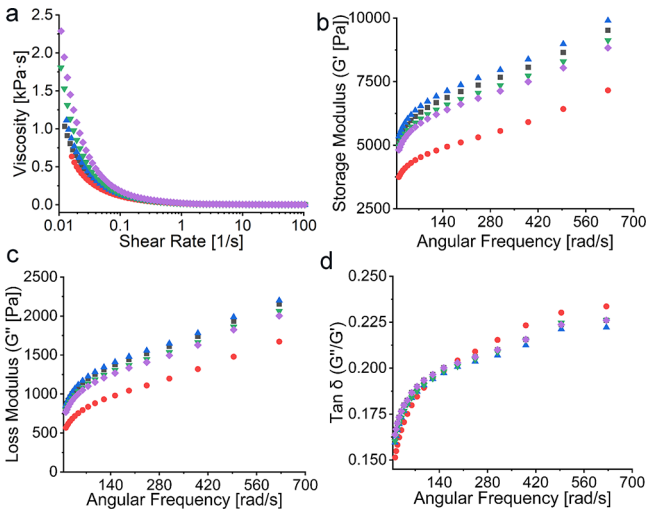

Figure 2. Rheology data of CNF-CLP0 (■ black), CNFCLP1 (● red), CNF-CLP5 (▲ blue), CNF-CLP10 (▼ green), and CNF-CLP25 (◆ purple): (a) Dynamic viscosity curves of all the biomaterial ink formulations with shearing rate ranging from 0 to 100 1/s; (b) storage modulus G′ and (c) loss modulus G′′ of all the biomaterial inks formulations; (d) Tan δ (G′′/G′).

most striking effect of the CLPs on the viscosity was an increase in zero shear rate viscosity as a function of CLP concentration. The only exception was CNF-CLP1, which may have exhibited lower viscosity due to the sliding effects with the low concentration of CLPs.[47] This increase in zero shear rate viscosity may have a positive effect on the printing resolution and shape fidelity of printed scaffolds. In a very recent publication on multifunctional membranes, Cusola et al. indicated indirectly that addition of lignin nanoparticles to CNF increased the viscosity of CNF gels.[50] However, the viscosity of the mixtures was not shown. In general, the viscosity of CNF-containing hydrogels with solid contents lower than 4% have been found to depend on the CNF concentration and not so much on soluble compounds like pectin[51] or alginate.[52] Tan (δ), which refers to the ratio between the loss modulus (G′′) and the storage modulus (G′), is depicted in Figure 2d, as a function of angular frequency. The obtained tan (δ) values of less than 1 indicate that all the biomaterial inks had a gel-like nature, suggesting high stability.[18] The storage modulus G′ and the loss modulus G′′ of CNF-alginate presented in Figure 2b,c were similar to previously published results.[18] In addition, CLPs did not change the loss or storage modulus for any of the formulated CNF-CLP biomaterial inks, except for CNF-CLP1. The storage modulus of the biomaterial inks were a few times higher than their loss modulus, which is expected to enable the biomaterial inks to recover their gel-like structure after cessation of shear and to maintain filament structure while printing.[21,53]

Antioxidant Properties of Biomaterial Inks. It is well-known that lignin has radical-scavenging ability,[54] which can be very useful for cell viability in wound-healing applications of the hydrogels as well as in general for the storage of the material. Figure 3 shows the antioxidant activity of model films

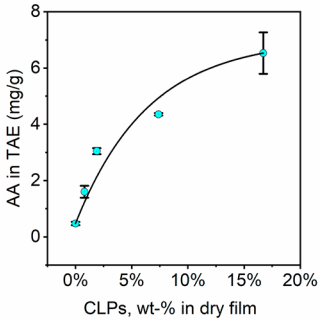

Figure 3. Antioxidant activity test of films produced from all CNF-alginate-CLP formulations with varying concentration of CLPs. Theoretical concentrations of CLPs in dry films were taken as *X* axis values.

prepared from the biomaterial ink hydrogels used in this work. The results are presented as milligrams of tannic acid equivalent per gram of dry sample film. We applied the method recently described by Farooq et al.[47] instead of the more commonly applied DPPH method to avoid solublization of lignin and to further illustrate the activity in a more natural environment. The DPPH method involves the use of ethanol or methanol as solvent. These solvents are rather good solvents for lignin, especially for the smaller molecules, and thus show the antioxidative activity of migrating molecules rather than that of the solid material. As expected, the antioxidant activity (AA) increased as the CLP concentration of the hydrogel increased. The antioxidant activity increased from 0.48 mg TAE g^{-1} for reference sample (CNF-alginate film without any lignin) to 6.53 mg TAE g^{-1} for the sample containing 16.7 wt % of CLPs. These values are 5 times higher than the AA previously measured in CNF-CLP nanocomposite membranes, but the shapes of the curves appear similar.[47] One reason for the increased AA values could be the difference in the film preparation methods. CNF-CLP suspensions were filtrated and then pressed to prepare CNF-CLP nanocomposite membranes in the previously reported work, leading to denser CNF-CLP nanocomposite membranes and possible loss of material during filtration. In contrast, the present model films, made from CNF-alginate-CLP, were dried at 23 °C without pressing or filtration. The observed nonlinear correlation could result from the increased diffusion barrier[47] caused by incremental changes of film microstructure with increasing content of CLPs. In most previous works, the activity is due to soluble lignin,[33,55] while in the present work, the lignin is in the form

https://dx.doi.org/10.1021/acs.biomac.9b01745
Biomacromolecules 2020, 21, 1875−1885

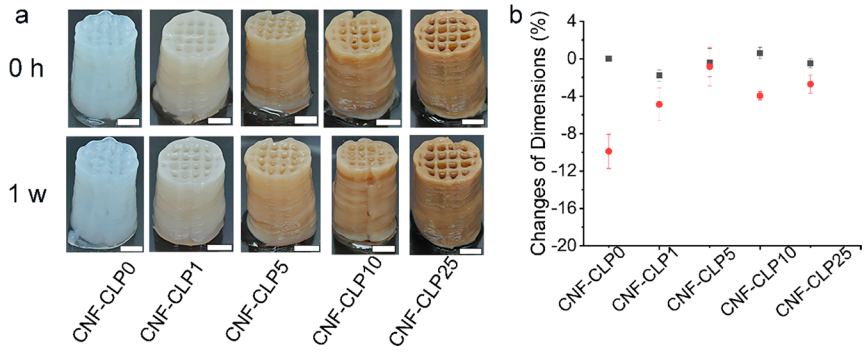

Figure 4. (a) The printed scaffolds immediately after cross-linking (0 h) and after storage in DPBS+ (1 week). Scale bars are 0.5 cm. (b) The corresponding dimensional change ratio in height (■ black) and cross-section (● red) of printed scaffolds were measured immediately after cross-linking and after 1 week of storage in DPBS+. The dimension changes were calculated for two scaffolds, and the error bars represent the average of the absolute deviations relative to the mean value (N = 2). All the scaffolds were printed into a cylinder shape with a diameter of 1.5 cm and a height of 2 cm.

of water-stable particles that are entrapped in the solid CNF-alginate matrix. This makes direct comparisons difficult. When we divided the highest antioxidant activity by the lignin concentration in that sample (6.53 mg/g divided by 16.7%), we obtained a value of 39 mg TAE g^{-1} for the antioxidant activity per gram lignin. A reference sample of CLPs' water dispersion possessed antioxidant activity around 75 mg TAE g^{-1}, which is roughly double the value in the dried samples. This confirms our hypothesis of diffusion effect on antioxidant properties of films containing CLPs. The observed nonzero antioxidant activity of CNF-alginate film (around 0.48 mg TAE g^{-1}) is due to the weak antioxidant activity of the alginate. The antioxidant ability of alignate is explained by the scavenging effect of hydroxyl radicals.[56]

Characterization of 3D-Printed Scaffolds. *Printability and Shape Fidelity.* The resolution and precision of scaffold structures, namely printability, is critical to consider when selecting suitable scaffold materials. More distinctly visible grid lines were observed in the printed scaffolds with an increasing concentration of CLPs. This indicates that the inclusion of the submicrometer-sized lignin particles had a positive effect on the printing resolution (Figure 4a,b). The results are well in line with the rheological properties of the biomaterial inks. The viscosity at zero shear rate of the biomaterial inks increased with increasing concentration of CLPs (Figure 2a,d), and accordingly, scaffolds could be printed with biomaterial inks containing larger amounts of CLPs. We can only hypothesize on the reason for the better printing resolution. One reason may be the ability of CLPs to form hydrogen bonds with CNF,[47,52] enabling the spherical particles to physically stabilize the CNF network and possibly also to avoid the aggregation of CNF fibrils that could occur due to extrusion forces during printing.

Shape fidelity is another important aspect to take into account when considering suitable applications for hydrogels. The more stable the structure, the easier its storage is. In the present work, the shape stability of non-cross-linked scaffolds (Figure S1a,c) and scaffolds cross-linked in $CaCl_2$ (Figure S1b,d and Figure 4a,b) were tested. No significant differences were found between the scaffolds that were not cross-linked. All samples showed some dimensional changes after 2 h, which are not apparent from the photos (Figure S1a,c). In this case, drying of the samples had a major effect on the dimensional changes. The relative dimensional changes of cross-linked samples which were stored at ambient conditions (Figure S1b) did not show sufficient improvement of shape stability in comparison with non-cross-linked samples. In contrast, the cross-linked scaffolds stored in 1× DPBS+ buffer solution for 1 week showed very minor changes. There was a clear improvement in shape fidelity caused by the addition of CLPs, particularly in the width. We can speculate that cross-linking had the largest effect on the shape stability of scaffolds containing CLPs because of the formation of ionic bonds not only between Ca^{2+} ions and the carboxyl groups of alginate but also between Ca^{2+} and the carboxyl groups of CLPs. Comparing the zeta potentials of CLPs (−37 mV) with the reported zeta potential of CNF at similar conditions and prepared from similar pulp (−3 mV)[57] suggests that CLPs have more carboxylic groups on the surface available for cross-linking with Ca^{2+} than CNF. Compared with previously reported results using CNF and alginate, we note that not all authors study the shape fidelity in buffer solution.[52,58,59] However, in general, our results are very good in comparison, and the printing resolution is very high.

Unconfined Compression. The mechanical properties of the materials have pronounced effects on the cell behavior in cell cultures. For instance, different mechanical stiffnesses may induce different phenotypes of cells or lead to a varied growth rate.[60,61] The compression test shown in Figure S3 revealed that the compression moduli did not show pronounced dependence on the concentration of CLPs. One possible explanation is that Ca^{2+} and Mg^{2+} from 1× DPBS+ buffer solution cross-linked the carboxyl groups from both alginate and CLPs, weakening the influence of CLPs. It is also assumed that hydrogen bonds between CLPs and CNF replace part of the interfibrillar hydrogen bonds of CNF. It was demonstrated by Aarstad et al. that the Young's modulus varies with the origins and relative amounts of CNF and alginate.[52,62] Alginate with more α-L-guluronic acid (G-block) and TEMPO-oxidized CNF improved the stiffness more than alginate with a higher amount of β-D-mannuronic acid (M block) or mechanically disintegrated CNF with lower charge. The reason was the increased amount of carboxylic groups providing more cross-linking sites for Ca^{2+}. A tunable Young's modulus of CNF-alginate scaffolds between 30 and 150 kPa was reported.[62] The results are much higher than 1.3−1.5 kPa observed here. A possible reason for this is the lower amount of alginate used in our biomaterial inks (0.5 wt % compared with around 1 wt %) and the use of unmodified, low charged CNF that contained fewer cross-linking sites. It is important to note that the moduli

https://dx.doi.org/10.1021/acs.biomac.9b01745
Biomacromolecules 2020, 21, 1875−1885

that we found ranging from 1.3 ± 0.21 kPa to 1.5 ± 0.14 kPa are suitable for the growth of liver cells.[63] The increase in viscosity induced by CLPs (and the associated enhancement of printability) without significantly changing the compression strength of the hydrogels is an important advantage for the use of CNF-alginate-CLP scaffolds in 3D cell cultures.

Rehydration Behavior of Scaffolds. Swelling properties were investigated to evaluate the ability of the hydrogels to adsorb water or aqueous buffer after drying. The swelling ability usually correlates with hydrophilicity, pore sizes, and density of scaffolds.[4] The hydroxyl, carboxyl groups, and other polar groups present on polysaccharides are capable of forming hydrogen bonds with water, which affect the water uptake degree.[64] In addition, the polysaccharide chains may form fibril networks which can entrap water in the voids.[59,65] Swelling properties affect cell behavior in the printed scaffold. It is known that CNF forms very strong hydrogen bonds upon drying, efficiently reducing the ability to rehydrate CNF hydrogels that have been dried. However, because of the presence of alginate and cross-linking, all hydrogels were efficiently rewetted. The dried CNF-alginate scaffolds were capable to take up around 30 times their own weight of water (Figure S2). The results are lower compared with the reported water uptake capacity of TEMPO-oxidized CNF aerogel (90 times of its dry weight),[66,67] likely because the interconnection of alginate with CNF and cross-linking will lead to a denser structure with a lower water uptake capacity.[68] The different CLP concentrations did not influence the rewetting properties of the hydrogels (Figure S2). All the scaffolds were capable of rehydrating to more than 80% of their starting weight (Figure 5). A slight reduction in the rehydration capability of CLP

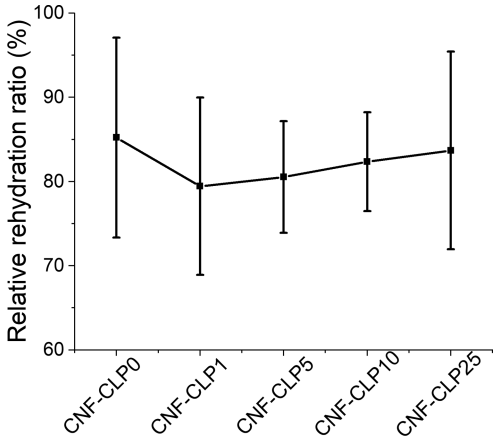

Figure 5. Relative rehydration ratios of freeze-dried scaffolds from different formulations, obtained through dividing the weight of rewetted scaffolds by the weight of the initial printed wet scaffolds. For each formulation, four scaffolds were measured, and the mean values were plotted. All the scaffolds were printed into a cylinder shape with a diameter of 8 mm and a height of 3 mm.

containing scaffolds was observed. It is postulated that due to the presence of considerable amount of carboxyl, aliphatic and phenolic hydroxyl groups at the surface of CLPs, they can efficiently form hydrogen bonds with CNF.[47,50] This reduces the number of the hydrogen bonds between CNF and water, correspondingly reducing swelling and producing more dense structures.[64] The high relative rehydration ratio will benefit not only storage and transportation of scaffolds but also sterilization, enabling tuning of the moisture content and further cell culture applications.[69]

Biocompatibility of 3D-Printed Scaffolds. Biocompatibility is essential for biomaterials. Trypan blue staining assay, where dead cells take up the dye and show blue color, indicated that the initial HepG2 viability prior to seeding was above 90%. HepG2 cells seeded on CNF-CLP0, CNF-CLP1, CNF-CLP5, CNF-CLP10, and CNF-CLP25 scaffolds were assessed by WST-1 assay for 5 days to monitor the cell viability and proliferation. Liver cells are sensitive to toxins; hence, we chose those to demonstrate biocompatibility of the material.[70] Fibroblast or myoblast cell lines are more commonly used, but they are actually very robust and do not show how well the material would work inside the body.[69,71] CNF-alginate-based biomaterial inks have been tested previously and displayed good biocompatibility with living human nasoseptal chondrocytes cells (hNC) and human bone-marrow-derived mesenchymal stem cells (hBM-MSC).[20,72,73] Hence, the cell viability of CNF-CLP0 was regarded as a reference in this work, and the effect of CLPs was compared to the biomaterial ink without CLPs. The proliferation data shown in Figure 6

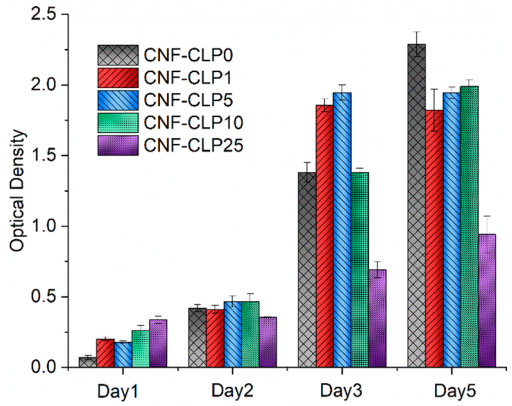

Figure 6. Biocompatibility test and HepG2 proliferation on scaffolds on day 1, day 2, day 3, and day 5.

indicates that all the formulated scaffolds exhibited good biocompatibility and favored extensive cell proliferation. The following trend was obtained from the optical density (OD_{460}) values shown in Figure 6, indicating the proliferation rate. On day 1, HepG2 attached on the surface of scaffolds. On day 2, cells started spreading and growing, and a double number of cells were obtained for all the formulated scaffold except for CNF-CLP25 well in line with the observed HepG2 proliferation time in complete cell medium.[74] Cell attachment and spreading are prerequisites for cell growth. Sufficiently high porosity is essential for cell spreading and nutrient transport to the cells. The dense structures of CNF-CLP25 demonstrated lower cell proliferation rate than the other biomaterial inks.

While the proliferation data obtained by WST-1 assay clearly showed the overall increase in proliferation rate quantitatively as a function of time, it does not provide evidence of the spatial location of cellular proliferation inside the scaffolds. For this reason, fluorescence microscopy was used to qualitatively study the growth of HepG2 cells inside the scaffolds. Because of the dense network of CNF and large height of the scaffolds, phase contrast and bright field imaging did not allow observations of cell growth inside the scaffold (Figure 7a). For this reason, we

https://dx.doi.org/10.1021/acs.biomac.9b01745
Biomacromolecules 2020, 21, 1875−1885

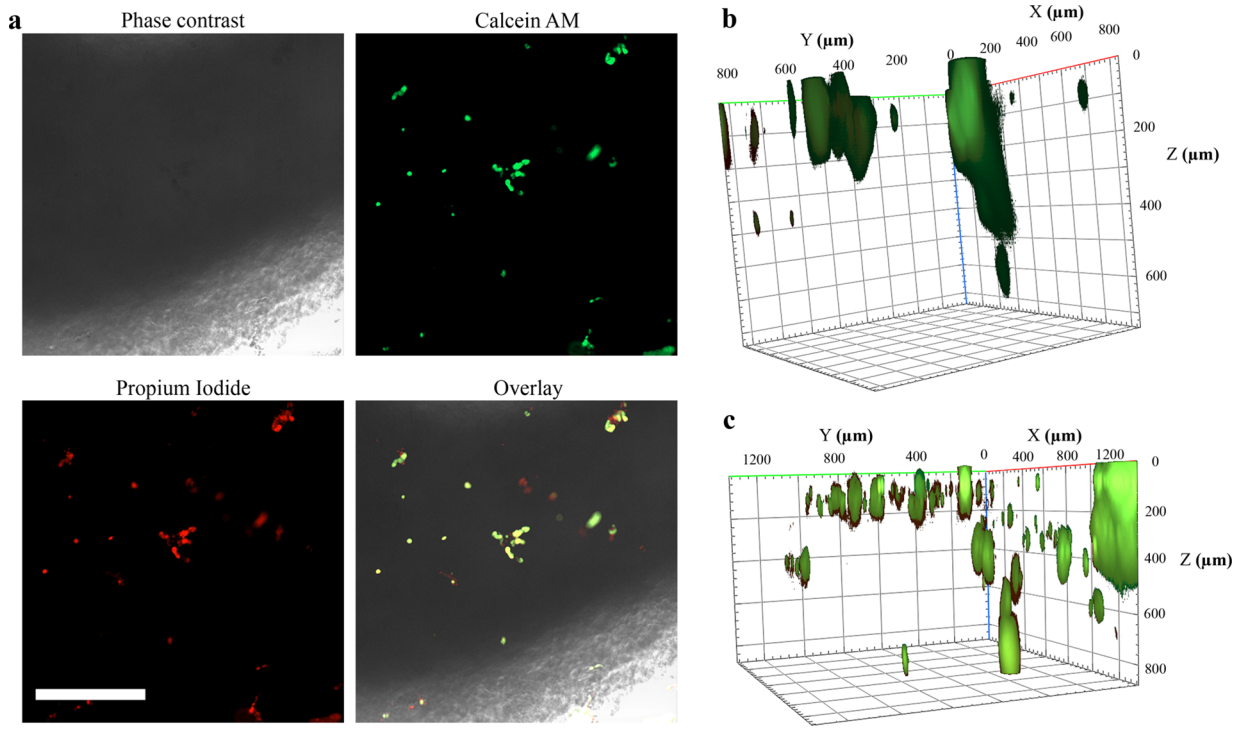

Figure 7. HepG2 cells inside CNF-alginate-CLPs based printed scaffolds. (a) Microscopy images of CNF-CLP25 scaffolds after 1 day of incubation. Phase-contrast image, focused on the edge of the scaffold, displays the poor light permeability of the scaffolds. However, Calcein AM and PI staining enabled monitoring of cellular growth inside the scaffolds. Scale bar is 200 μm. (b) 3D reconstruction from Calcein AM and PI staining Z-stacks (5 μm spacing) of a CNF-CLP25 scaffold after 1 day of incubation, which displays the attachment of HepG2 cells mostly in a horizontal direction. (c) 3D reconstruction from Calcein AM and PI staining Z-stacks (5 μm spacing) of a CNF-CLP25 scaffold after 5 days of incubation, which displays the growth of HepG2 cells in a horizontal and vertical direction.

used fluorescence staining with calcein-AM and propidium iodide (PI), which enabled the monitoring of HepG2 cells over longer periods of time inside the scaffolds. The overlaid images indicated the specificity of the stains for HepG2 cells, since the CNF-alginate-CLP scaffolds did not display any detectable interfering fluorescence signal. A 3D reconstruction of Z-stack images in Figure 7b,c shows that the analysis of cellular growth and viability is possible until at least 800 μm (*Z*-direction). This enabled us to monitor the growth inside the scaffolds.

The 3D reconstruction of HepG2 cells inside a CNF-CLP25 scaffold 1 day after printing shows that cells attached to the scaffold (Figure 7b). Although some cells clearly penetrated into the scaffolding structure, the majority of cells were found at the surface. In a similar 3D reconstruction after 5 days (Figure 7c), a significantly increased fluorescence signal was detected. We also observed an increase of cells present at different heights (*Z*-directions). This indicates that proliferation of cells occurs not only on the surfaces but also inside the scaffolding structure. It must be further noted that those images were taken for the scaffolds with the highest CLPs content.

We then studied the effects of increasing concentrations of CLPs in the scaffolds on HepG2 cellular growth over a period of up to 5 days. The increasing density of live cells (in green) indicate that the scaffolds are biocompatible and enable cellular proliferation (Figure 8). We did not detect any decrease in cell compatibility associated with the CLP concentrations. The cell density increased from day 1 to day 2 and day 5 in all the scaffolds.

As observed above in Figure 8, the cell growth was not hampered by CLPs. This agreed with the previous finding by

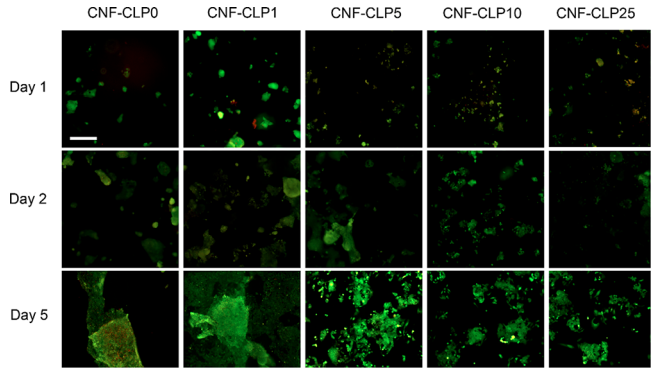

Figure 8. Fluorescence microscopy images of HepG2 cells, seeded on the formulated scaffolds, after 1 day, 2 days, and 5 days of incubation, with increasing relative concentrations of lignin to dry CNF (from 0 to 25%). Scale bar, 100 μm.

Gan et al., who found that lignin particles do not cause adverse effects on the biocompatibility of LNP-pectin-poly(acrylic acid) hydrogel.[42] Interestingly, an increase in red PI fluorescence signal, associated with dead cells, was detected in all samples at day 1, most prominently in sample CNF-CLP1. The seeding, handling, and loading of HepG2 cells on scaffolds results in physical forces that are known to induce cellular stress and, in some cases, cell death.[75,76] This could partially explain the presence of small amounts of PI-stained cells after the first day. On day 2, however, the PI signal is absent in all samples, and an overall increase in cell density was observed in all scaffold samples, indicating that the scaffolds have a positive effect on cell attachment and proliferation.

https://dx.doi.org/10.1021/acs.biomac.9b01745
Biomacromolecules 2020, 21, 1875−1885

These phenomena imply that CLP-containing porous, hydrophilic, and mesh-like scaffolds with large surface area have great potential for biomedical applications requiring tailorable 3D cell culture scaffolds.

CONCLUSIONS

In the current work, CLPs have been used for the first time to tune the properties of hydrogels for 3D printing. The novel CLP-containing biomaterial inks, consisting of CNF, alginate, and CLPs, demonstrated excellent properties for 3D printing. A relative concentration of CLPs to dry CNF up to 25% did not alter the shear-thinning behavior, an essential property for 3D printing of biomaterial inks, whereas it did result in an improved printing resolution. The addition of CLPs furthermore brought beneficial antioxidant properties to the biomaterial inks and improved the shape fidelity of the printed scaffolds, since CLPs provide additional cross-linking sites for divalent ions which are also present in cell culture media. It was found that all the formulated scaffolds had high swelling ratios, indicating a good capability to retain and adsorb water. In addition, the consistent growth of HepG2 in all the formulated scaffolds demonstrated their good biocompatibility, regardless of the CLP content. Overall, the findings indicated that CLP-containing scaffolds are good candidates in soft tissue engineering applications and hold potential for use in regenerative medicine.

ASSOCIATED CONTENT

Supporting Information

The Supporting Information is available free of charge at https://pubs.acs.org/doi/10.1021/acs.biomac.9b01745.

Dimensional change ratio of printed scaffolds after storage at ambient conditions for 2 h and corresponding photos of the printed scaffolds (Figure S1). Swelling ratio behavior of freeze-dried scaffolds of different formulations (Figure S2). Compressive Young's modulus of printed solid constructs of 100% infill of different formulations Compressive Young's modulus of printed solid constructs of 100% infill of different formulations after storage in 1× DPBS+ for 48 h (Figure S3) (PDF)

AUTHOR INFORMATION

Corresponding Author

Monika Österberg − *Department of Bioproducts and Biosystems, School of Chemical Engineering, Aalto University, FI-00076 Aalto, Finland;* orcid.org/0000-0002-3558-9172; Phone: +358505497218; Email: monika.osterberg@aalto.fi

Authors

Xue Zhang − *Department of Bioproducts and Biosystems, School of Chemical Engineering, Aalto University, FI-00076 Aalto, Finland;* orcid.org/0000-0002-7476-5167

Maria Morits − *Department of Bioproducts and Biosystems, School of Chemical Engineering, Aalto University, FI-00076 Aalto, Finland;* orcid.org/0000-0002-0972-182X

Christopher Jonkergouw − *Department of Bioproducts and Biosystems, School of Chemical Engineering, Aalto University, FI-00076 Aalto, Finland*

Ari Ora − *Department of Applied Physics, School of Science, Aalto University, FIN-02150 Espoo, Finland*

Juan José Valle-Delgado − *Department of Bioproducts and Biosystems, School of Chemical Engineering, Aalto University, FI-00076 Aalto, Finland;* orcid.org/0000-0002-4808-1730

Muhammad Farooq − *Department of Bioproducts and Biosystems, School of Chemical Engineering, Aalto University, FI-00076 Aalto, Finland*

Rubina Ajdary − *Department of Bioproducts and Biosystems, School of Chemical Engineering, Aalto University, FI-00076 Aalto, Finland*

Siqi Huan − *Department of Bioproducts and Biosystems, School of Chemical Engineering, Aalto University, FI-00076 Aalto, Finland*

Markus Linder − *Department of Bioproducts and Biosystems, School of Chemical Engineering, Aalto University, FI-00076 Aalto, Finland;* orcid.org/0000-0002-7271-6441

Orlando Rojas − *Department of Bioproducts and Biosystems, School of Chemical Engineering, Aalto University, FI-00076 Aalto, Finland;* orcid.org/0000-0003-4036-4020

Mika Henrikki Sipponen − *Department of Bioproducts and Biosystems, School of Chemical Engineering, Aalto University, FI-00076 Aalto, Finland;* orcid.org/0000-0001-7747-9310

Complete contact information is available at: https://pubs.acs.org/10.1021/acs.biomac.9b01745

Author Contributions

X.Z. designed the experiments together with M.M., M.H.S., and M.Ö. Experiments and data analysis were performed by X.Z and M.M. in collaboration with M.H.S. and M.Ö. M.M. contributed to the CLPs preparation and characterization with the input of M.H.S. M.M conducted the shape fidelity test and antioxidant characterization. C.J. took the fluorescence images and wrote the corresponding parts in the manuscript. X.Z wrote the manuscript with input from all authors. M.F prepared the schematic figure and abstract image. All authors discussed the results and read and approved the manuscript.

Notes

The authors declare no competing financial interest.

ACKNOWLEDGMENTS

Authors acknowledge M.Sc. Teemu Välisalmi for valuable discussions and assistance on the cell viability test, M.Sc. Riviere Guillaume for assistance on the antioxidant activity test, and M.Sc. Laura Äkräs for preliminary experiments. X.Z. is grateful for the support by the FinnCERES Materials Bioeconomy Ecosystem, while preparing the manuscript. This work made use of Aalto University Bioeconomy Facilities.

REFERENCES

(1) Chun, H. J.; Park, K.; Kim, C.-H.; Khang, G. *Novel Biomaterials for Regenerative Medicine*; Springer, Singapore: Singapore, 2018.

(2) Tibbitt, M. W.; Anseth, K. S. Hydrogels as Extracellular Matrix Mimics for 3D Cell Culture. *Biotechnol. Bioeng.* **2009**, *103*, 655−663.

(3) Gaspar, V. M.; Lavrador, P.; Borges, J.; Oliveira, M. B.; Mano, J. F. Advanced Bottom-up Engineering of Living Architectures. *Adv. Mater.* **2019**, 1903975.

(4) Caliari, S. R.; Burdick, J. A. A Practical Guide to Hydrogels for Cell Culture. *Nat. Methods* **2016**, *13* (5), 405−414.

(5) De France, K. J.; Badv, M.; Dorogin, J.; Siebers, E.; Panchal, V.; Babi, M.; Moran-Mirabal, J.; Lawlor, M.; Cranston, E. D.; Hoare, T. Tissue Response and Biodistribution of Injectable Cellulose Nanocrystal Composite Hydrogels. *ACS Biomater. Sci. Eng.* **2019**, *5* (5), 2235−2246.

(6) Wang, Y. K.; Chen, C. S. Cell Adhesion and Mechanical Stimulation in the Regulation of Mesenchymal Stem Cell Differentiation. *J. Cell. Mol. Med.* **2013**, *17* (7), 823−832.
(7) Bhattacharya, M.; Malinen, M. M.; Lauren, P.; Lou, Y. R.; Kuisma, S. W.; Kanninen, L.; Lille, M.; Corlu, A.; Guguen-Guillouzo, C.; Ikkala, O.; Laukkanen, A.; Urtti, A.; Yliperttula, M. Nanofibrillar Cellulose Hydrogel Promotes Three-Dimensional Liver Cell Culture. *J. Controlled Release* **2012**, *164* (3), 291−298.
(8) Walther, A.; Timonen, J. V. I.; Díez, I.; Laukkanen, A.; Ikkala, O. Multifunctional High-Performance Biofibers Based on Wet-Extrusion of Renewable Native Cellulose Nanofibrils. *Adv. Mater.* **2011**, *23* (26), 2924−2928.
(9) Harjumäki, R.; Nugroho, R. W. N.; Zhang, X.; Lou, Y. R.; Yliperttula, M.; Valle-Delgado, J. J.; Österberg, M. Quantified Forces between HepG2 Hepatocarcinoma and WA07 Pluripotent Stem Cells with Natural Biomaterials Correlate with in Vitro Cell Behavior. *Sci. Rep.* **2019**, *9* (1), 1−14.
(10) Laurén, P.; Lou, Y. R.; Raki, M.; Urtti, A.; Bergström, K.; Yliperttula, M. Technetium-99m-Labeled Nanofibrillar Cellulose Hydrogel for in Vivo Drug Release. *Eur. J. Pharm. Sci.* **2014**, *65* (2014), 79−88.
(11) Xu, W.; Molino, B. Z.; Cheng, F.; Molino, P. J.; Yue, Z.; Su, D.; Wang, X.; Willför, S.; Xu, C.; Wallace, G. G. On Low-Concentration Inks Formulated by Nanocellulose Assisted with Gelatin Methacrylate (GelMA) for 3D Printing toward Wound Healing Application. *ACS Appl. Mater. Interfaces* **2019**, *11* (9), 8838−8848.
(12) Xu, C.; Zhang Molino, B.; Wang, X.; Cheng, F.; Xu, W.; Molino, P.; Bacher, M.; Su, D.; Rosenau, T.; Willför, S.; Wallace, G. 3D Printing of Nanocellulose Hydrogel Scaffolds with Tunable Mechanical Strength towards Wound Healing Application. *J. Mater. Chem. B* **2018**, *6*, 7066−7075.
(13) Ilkhanizadeh, S.; Teixeira, A. I.; Hermanson, O. Inkjet Printing of Macromolecules on Hydrogels to Steer Neural Stem Cell Differentiation. *Biomaterials* **2007**, *28*, 3936−3943.
(14) Xu, W.; Wang, X.; Sandler, N.; Willför, S.; Xu, C. Three-Dimensional Printing of Wood-Derived Biopolymers: A Review Focused on Biomedical Applications. *ACS Sustainable Chem. Eng.* **2018**, *6* (5), 5663−5680.
(15) Håkansson, K. M. O.; Henriksson, I. C.; de la Peña Vázquez, C.; Kuzmenko, V.; Markstedt, K.; Enoksson, P.; Gatenholm, P. Solidification of 3D Printed Nanofibril Hydrogels into Functional 3D Cellulose Structures. *Adv. Mater. Technol.* **2016**, *1* (7), 1600096.
(16) Henriksson, I.; Gatenholm, P.; Hägg, D. A. Increased Lipid Accumulation and Adipogenic Gene Expression of Adipocytes in 3D Bioprinted Nanocellulose Scaffolds. *Biofabrication* **2017**, *9*, 015022.
(17) Wang, B.; Benitez, A. J.; Lossada, F.; Merindol, R.; Walther, A. Bioinspired Mechanical Gradients in Cellulose Nanofibril/Polymer Nanopapers. *Angew. Chem., Int. Ed.* **2016**, *55*, 5966−5970.
(18) Markstedt, K.; Mantas, A.; Tournier, I.; Martínez Ávila, H.; Hägg, D.; Gatenholm, P. 3D Bioprinting Human Chondrocytes with Nanocellulose-Alginate Bioink for Cartilage Tissue Engineering Applications. *Biomacromolecules* **2015**, *16* (5), 1489−1496.
(19) Pfister, A.; Landers, R.; Laib, A.; Hübner, U.; Schmelzeisen, R.; Mülhaupt, R. Biofunctional Rapid Prototyping for Tissue-Engineering Applications: 3D Bioplotting versus 3D Printing. *J. Polym. Sci., Part A: Polym. Chem.* **2004**, *42* (3), 624−638.
(20) Markstedt, K.; Escalante, A.; Toriz, G.; Gatenholm, P. Biomimetic Inks Based on Cellulose Nanofibrils and Cross-Linkable Xylans for 3D Printing. *ACS Appl. Mater. Interfaces* **2017**, *9*, 40878−40886.
(21) Huan, S.; Ajdary, R.; Bai, L.; Klar, V.; Rojas, O. J. Low Solids Emulsion Gels Based on Nanocellulose for 3D-Printing. *Biomacromolecules* **2019**, *20* (2), 635−644.
(22) Groll, J.; Burdick, J. A.; Cho, D. W.; Derby, B.; Gelinsky, M.; Heilshorn, S. C.; Jüngst, T.; Malda, J.; Mironov, V. A.; Nakayama, K.; Ovsianikov, A.; Sun, W.; Takeuchi, S.; Yoo, J. J.; Woodfield, T. B. F. A Definition of Bioinks and Their Distinction from Biomaterial Inks. *Biofabrication* **2019**, *11* (1), 013001.
(23) Axpe, E.; Oyen, M. Applications of Alginate-Based Bioinks in 3D Bioprinting. *Int. J. Mol. Sci.* **2016**, *17* (12), 1976−1987.
(24) Lee, K. Y.; Mooney, D. J. Alginate: Properties and Biomedical Applications. *Prog. Polym. Sci.* **2012**, *37* (1), 106−126.
(25) Siqueira, P.; Siqueira, É.; de Lima, A. E.; Siqueira, G.; Pinzón-Garcia, A. D.; Lopes, A. P.; Segura, M. E. C.; Isaac, A.; Pereira, F. V.; Botaro, V. R. Three-Dimensional Stable Alginate-Nanocellulose Gels for Biomedical Applications: Towards Tunable Mechanical Properties and Cell Growing. *Nanomaterials* **2019**, *9* (1), 78.
(26) Norgren, M.; Edlund, H. Lignin: Recent Advances and Emerging Applications. *Curr. Opin. Colloid Interface Sci.* **2014**, *19* (5), 409−416.
(27) Witzler, M.; Alzagameem, A.; Bergs, M.; Khaldi-Hansen, B. El; Klein, S. E.; Hielscher, D.; Kamm, B.; Kreyenschmidt, J.; Tobiasch, E.; Schulze, M. Lignin-Derived Biomaterials for Drug Release and Tissue Engineering. *Molecules* **2018**, *23* (8), 1885−1907.
(28) Reesi, F.; Minaiyan, M.; Taheri, A. A Novel Lignin-Based Nanofibrous Dressing Containing Arginine for Wound-Healing Applications. *Drug Delivery Transl. Res.* **2018**, *8* (1), 111−122.
(29) Crestini, C.; Lange, H.; Sette, M.; Argyropoulos, D. S. On the Structure of Softwood Kraft Lignin. *Green Chem.* **2017**, *19* (17), 4104−4121.
(30) Tardy, B. L.; Richardson, J. J.; Guo, J.; Lehtonen, J.; Ago, M.; Rojas, O. J. Lignin Nano- and Microparticles as Template for Nanostructured Materials: Formation of Hollow Metal-Phenolic Capsules. *Green Chem.* **2018**, *20* (6), 1335−1344.
(31) Quraishi, S.; Martins, M.; Barros, A. A.; Gurikov, P.; Raman, S. P.; Smirnova, I.; Duarte, A. R. C.; Reis, R. L. Novel Non-Cytotoxic Alginate−Lignin Hybrid Aerogels as Scaffolds for Tissue Engineering. *J. Supercrit. Fluids* **2015**, *105*, 1−8.
(32) Kai, D.; Low, Z. W.; Liow, S. S.; Abdul Karim, A.; Ye, H.; Jin, G.; Li, K.; Loh, X. J. Development of Lignin Supramolecular Hydrogels with Mechanically Responsive and Self-Healing Properties. *ACS Sustainable Chem. Eng.* **2015**, *3*, 2160−2169.
(33) Kai, D.; Zhang, K.; Jiang, L.; Wong, H. Z.; Li, Z.; Zhang, Z.; Loh, X. J. Sustainable and Antioxidant Lignin-Polyester Copolymers and Nanofibers for Potential Healthcare Applications. *ACS Sustainable Chem. Eng.* **2017**, *5*, 6016−6025.
(34) Domínguez-Robles, J.; Martin, N. K.; Fong, M. L.; Stewart, S. A.; Irwin, N. J.; Rial-Hermida, M. I.; Donnelly, R. F.; Larrañeta, E. Antioxidant Pla Composites Containing Lignin for 3D Printing Applications: A Potential Material for Healthcare Applications. *Pharmaceutics* **2019**, *11* (4), 165.
(35) Sipponen, M. H.; Lange, H.; Ago, M.; Crestini, C. Understanding Lignin Aggregation Processes. A Case Study: Budesonide Entrapment and Stimuli Controlled Release from Lignin Nanoparticles. *ACS Sustainable Chem. Eng.* **2018**, *6* (7), 9342−9351.
(36) Lievonen, M.; Valle-Delgado, J. J.; Mattinen, M. L.; Hult, E. L.; Lintinen, K.; Kostiainen, M. A.; Paananen, A.; Szilvay, G. R.; Setälä, H.; Österberg, M. A Simple Process for Lignin Nanoparticle Preparation. *Green Chem.* **2016**, *18* (5), 1416−1422.
(37) Henn, A.; Mattinen, M.-L. Valued Applications of Lignin Nanoparticles. *Recent Prog. Mater.* **2019**, *1* (2), 1−1.
(38) Mattinen, M. L.; Riviere, G.; Henn, A.; Nugroho, R. W. N.; Leskinen, T.; Nivala, O.; Valle-Delgado, J. J.; Kostiainen, M. A.; Österberg, M. Colloidal Lignin Particles as Adhesives for Soft Materials. *Nanomaterials* **2018**, *8* (12), 1001.
(39) Zou, T.; Sipponen, M. H.; Österberg, M. Natural Shape-Retaining Microcapsules with Shells Made of Chitosan-Coated Colloidal Lignin Particles. *Front. Chem.* **2019**, *7*, 370−382.
(40) Richter, A. P.; Brown, J. S.; Bharti, B.; Wang, A.; Gangwal, S.; Houck, K.; Cohen Hubal, E. A.; Paunov, V. N.; Stoyanov, S. D.; Velev, O. D. An Environmentally Benign Antimicrobial Nanoparticle Based on a Silver-Infused Lignin Core. *Nat. Nanotechnol.* **2015**, *10* (9), 817−823.
(41) Yang, W.; Owczarek, J. S.; Fortunati, E.; Kozanecki, M.; Mazzaglia, A.; Balestra, G. M.; Kenny, J. M.; Torre, L.; Puglia, D. Antioxidant and Antibacterial Lignin Nanoparticles in Polyvinyl

https://dx.doi.org/10.1021/acs.biomac.9b01745
Biomacromolecules 2020, 21, 1875−1885

Alcohol/Chitosan Films for Active Packaging. *Ind. Crops Prod.* **2016**, *94*, 800−811.
(42) Gan, D.; Xing, W.; Jiang, L.; Fang, J.; Zhao, C.; Ren, F.; Fang, L.; Wang, K.; Lu, X. Plant-Inspired Adhesive and Tough Hydrogel Based on Ag-Lignin Nanoparticles-Triggered Dynamic Redox Catechol Chemistry. *Nat. Commun.* **2019**, *10* (1), 1−10.
(43) Leskinen, T.; Witos, J.; Valle-Delgado, J. J.; Lintinen, K.; Kostiainen, M.; Wiedmer, S. K.; Österberg, M.; Mattinen, M. L. Adsorption of Proteins on Colloidal Lignin Particles for Advanced Biomaterials. *Biomacromolecules* **2017**, *18* (9), 2767−2776.
(44) Figueiredo, P.; Lintinen, K.; Kiriazis, A.; Hynninen, V.; Liu, Z.; Bauleth-Ramos, T.; Rahikkala, A.; Correia, A.; Kohout, T.; Sarmento, B.; Yli- Kauhaluoma, J.; et al. In Vitro Evaluation of Biodegradable Lignin-Based Nanoparticles for Drug Delivery and Enhanced Antiproliferation Effect in Cancer Cells. *Biomaterials* **2017**, *121*, 97−108.
(45) Sipponen, M. H.; Farooq, M.; Koivisto, J.; Pellis, A.; Seitsonen, J.; Österberg, M. Spatially confined lignin nanospheres for biocatalytic ester synthesis in aqueous media. *Nat. Commun.* **2018**, *9*, 1−7.
(46) Eronen, P.; Junka, K.; Laine, J.; Österberg, M. Interaction between Water-Soluble Polysaccharides and Native Nanofibrillar Cellulose Thin Films. *BioResources* **2011**, *6* (4), 4200−4217.
(47) Farooq, M.; Zou, T.; Riviere, G.; Sipponen, M. H.; Österberg, M. Strong, Ductile and Waterproof Cellulose Nanofibril Composite Films with Colloidal Lignin Particles. *Biomacromolecules* **2019**, *20* (2), 693−704.
(48) Ahola, S.; Salmi, J.; Johansson, L. S.; Laine, J.; Österberg, M. Model Films from Native Cellulose Nanofibrils. Preparation, Swelling, and Surface Interactions. *Biomacromolecules* **2008**, *9*, 1273−1282.
(49) Decho, A. W. Imaging an Alginate Polymer Gel Matrix Using Atomic Force Microscopy. *Carbohydr. Res.* **1999**, *315* (3−4), 330−333.
(50) Cusola, O.; Rojas, O. J.; Roncero, M. B. Lignin Particles for Multifunctional Membranes, Antioxidative Microfiltration, Patterning, and 3D Structuring. *ACS Appl. Mater. Interfaces* **2019**, *11* (48), 45226−45236.
(51) Cernencu, A. I.; Lungu, A.; Stancu, I. C.; Serafim, A.; Heggset, E.; Syverud, K.; Iovu, H. Bioinspired 3D Printable Pectin-Nanocellulose Ink Formulations. *Carbohydr. Polym.* **2019**, *220* (2019), 12−21.
(52) Heggset, E. B.; Strand, B. L.; Sundby, K. W.; Simon, S.; Chinga-Carrasco, G.; Syverud, K. Viscoelastic Properties of Nanocellulose Based Inks for 3D Printing and Mechanical Properties of CNF/Alginate Biocomposite Gels. *Cellulose* **2019**, *26* (1), 581−595.
(53) Compton, B. G.; Lewis, J. A. 3D-Printing of Lightweight Cellular Composites. *Adv. Mater.* **2014**, *26* (34), 5930−5935.
(54) Yearla, S. R.; Padmasree, K. Preparation and Characterisation of Lignin Nanoparticles: Evaluation of Their Potential as Antioxidants and UV Protectants. *J. Exp. Nanosci.* **2016**, *11* (4), 289−302.
(55) Núñez-Flores, R.; Giménez, B.; Fernández-Martín, F.; López-Caballero, M. E.; Montero, M. P.; Gómez-Guillén, M. C. Physical and Functional Characterization of Active Fish Gelatin Films Incorporated with Lignin. *Food Hydrocolloids* **2013**, *30* (1), 163−172.
(56) Sellimi, S.; Younes, I.; Ayed, H. B.; Maalej, H.; Montero, V.; Rinaudo, M.; Dahia, M.; Mechichi, T.; Hajji, M.; Nasri, M. Structural, Physicochemical and Antioxidant Properties of Sodium Alginate Isolated from a Tunisian Brown Seaweed. *Int. J. Biol. Macromol.* **2015**, *72*, 1358−1367.
(57) Eronen, P.; Laine, J.; Ruokolainen, J.; Österberg, M. Comparison of Multilayer Formation Between Different Cellulose Nanofibrils and Cationic Polymers. *J. Colloid Interface Sci.* **2012**, *373* (1), 84−93.
(58) Jessop, Z. M.; Al-Sabah, A.; Gao, N.; Kyle, S.; Thomas, B.; Badiei, N.; Hawkins, K.; Whitaker, I. S. Printability of Pulp Derived Crystal, Fibril and Blend Nanocellulose-Alginate Bioinks for Extrusion 3D Bioprinting. *Biofabrication* **2019**, *11* (4), 045006.
(59) Espinosa, E.; Filgueira, D.; Rodríguez, A.; Chinga-Carrasco, G. Nanocellulose-Based Inks—Effect of Alginate Content on the Water Absorption of 3D Printed Constructs. *Bioengineering* **2019**, *6* (3), 65−75.
(60) Jeong, J. H.; Liang, Y.; Jang, M.; Cha, C.; Chu, C.; Lee, H.; Jung, W.; Kim, J. W.; Boppart, S. A.; Kong, H. Stiffness-Modulated Water Retention and Neovascularization of Dermal Fibroblast-Encapsulating Collagen Gel. *Tissue Eng., Part A* **2013**, *19* (11−12), 1275−1284.
(61) Schrader, J.; Gordon-Walker, T. T.; Aucott, R. L.; van Deemter, M.; Quaas, A.; Walsh, S.; Benten, D.; Forbes, S. J.; Wells, R. G.; Iredale, J. P. Matrix Stiffness Modulates Proliferation, Chemotherapeutic Response, and Dormancy in Hepatocellular Carcinoma Cells. *Hepatology* **2011**, *53* (4), 1192−1205.
(62) Aarstad, O.; Heggset, E. B.; Pedersen, I. S.; Bjørnøy, S. H.; Syverud, K.; Strand, B. L. Mechanical Properties of Composite Hydrogels of Alginate and Cellulose Nanofibrils. *Polymers (Basel, Switz.)* **2017**, *9* (8), 378−397.
(63) Yeh, W.-C.; Li, P.-C.; Jeng, Y.-M.; Hsu, H.-C.; Kuo, P.-L.; Li, M.-L.; Yang, P.-M.; Lee, P. H. Elastic Modulus Measurements of Human Liver and Correlation with Pathology. *Ultrasound Med. Biol.* **2002**, *28* (4), 467−474.
(64) Kontturi, K. S.; Kontturi, E.; Laine, J. Specific Water Uptake of Thin Films from Nanofibrillar Cellulose. *J. Mater. Chem. A* **2013**, *1* (43), 13655−13663.
(65) Zhang, Z. S.; Wang, X. M.; Han, Z. P.; Zhao, M. X.; Yin, L. Purification, Antioxidant and Moisture-Preserving Activities of Polysaccharides from Papaya. *Carbohydr. Polym.* **2012**, *87* (3), 2332−2337.
(66) Liu, J.; Cheng, F.; Grénman, H.; Spoljaric, S.; Seppälä, J.; Eriksson, J. E.; Willför, S.; Xu, C. Development of Nanocellulose Scaffolds with Tunable Structures to Support 3D Cell Culture. *Carbohydr. Polym.* **2016**, *148* (2016), 259−271.
(67) Lin, N.; Bruzzese, C.; Dufresne, A. TEMPO-Oxidized Nanocellulose Participating as Crosslinking Aid for Alginate-Based Sponges. *ACS Appl. Mater. Interfaces* **2012**, *4* (9), 4948−4959.
(68) DeVos, P.; DeHaan, B.; Wolters, G. H. J.; VanSchilfgaarde, R. Factors Influencing the Adequacy of Microencapsulation of Rat Pancreatic Islets LK. *Transplantation* **1996**, *62* (7), 888−893.
(69) Ajdary, R.; Huan, S.; Zanjanizadeh Ezazi, N.; Xiang, W.; Grande, R.; Santos, H. A.; Rojas, O. J. Acetylated Nanocellulose for Single-Component Bioinks and Cell Proliferation on 3D-Printed Scaffolds. *Biomacromolecules* **2019**, *20* (7), 2770−2778.
(70) Mersch-Sundermann, V.; Knasmüller, S.; Wu, X. J.; Darroudi, F.; Kassie, F. Use of a Human-Derived Liver Cell Line for the Detection of Cytoprotective, Antigenotoxic and Cogenotoxic Agents. *Toxicology* **2004**, *198* (1−3), 329−340.
(71) Ichim, T. E.; O'Heeron, P.; Kesari, S. Fibroblasts as a Practical Alternative to Mesenchymal Stem Cells. *J. Transl. Med.* **2018**, *16* (1), 1−9.
(72) Apelgren, P.; Amoroso, M.; Säljö, K.; Lindahl, A.; Brantsing, C.; Stridh Orrhult, L.; Gatenholm, P.; Kölby, L. Skin Grafting on 3D Bioprinted Cartilage Constructs In Vivo. *Plast. Reconstr. Surg. - Glob. Open* **2018**, *6* (9), No. e1930.
(73) Martínez Avila, H.; Schwarz, S.; Rotter, N.; Gatenholm, P. 3D Bioprinting of Human Chondrocyte-Laden Nanocellulose Hydrogels for Patient-Specific Auricular Cartilage Regeneration. *Bioprinting* **2016**, *1*−*2*, 22−35.
(74) Norouzzadeh, M.; Kalikias, Y.; Mohamadpur, Z.; Sharifi, L. Determining Population Doubling Time and the Appropriate Number of HepG2 Cells for Culturing in 6- Well Plate. *Int. Res. J. Appl. Basic Sci.* **2016**, *10* (3), 299−303.
(75) Ziko, L.; Riad, S.; Amer, M.; Zdero, R.; Bougherara, H.; Amleh, A. Mechanical Stress Promotes Cisplatin-Induced Hepatocellular Carcinoma Cell Death. *BioMed Res. Int.* **2015**, *2015*, 430569.
(76) Mitchell, M. J.; King, M. R. Fluid Shear Stress Sensitizes Cancer Cells to Receptor-Mediated Apoptosis via Trimeric Death Receptors. *New J. Phys.* **2013**, *15*, 015008.

https://dx.doi.org/10.1021/acs.biomac.9b01745
Biomacromolecules 2020, 21, 1875−1885